ACS OMEGA

Open Access

http://pubs.acs.org/journal/acsodf

Article

Anisotropic Damage Mechanism of Coal Seam Water Injection with Multiphase Coupling

Yuehui Liang,* Biming Shi, Jiwei Yue, Chengcheng Zhang, and Qijun Han

Cite This: *ACS Omega* 2024, 9, 16400−16410

Read Online

ACCESS | Metrics & More | Article Recommendations

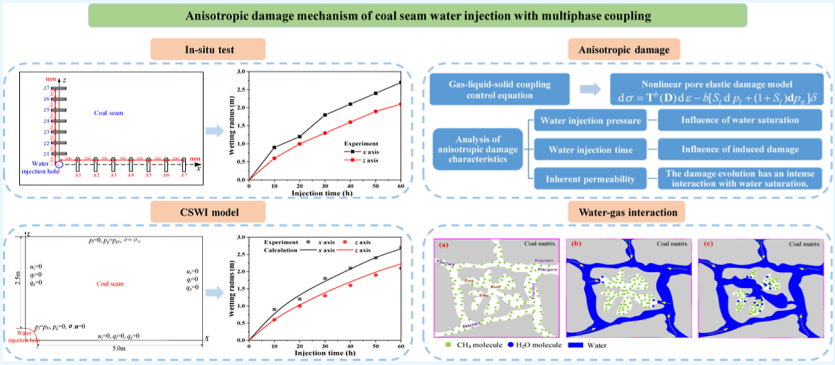

ABSTRACT: After coal seam water injection, coal mechanical properties will change with brittleness weakening and plasticity enhancement. Aiming at the problem of coal damage caused by the coal seam water injection process, based on nonlinear pore elasticity theory and continuum damage theory, a nonlinear pore elastic damage model considering anisotropic characteristics is proposed to calculate and analyze the gas−liquid−solid multiphase coupling effect with the fully coupled finite element method during the coal seam water injection process. The research results indicate that the wetting radius of calculated results by the model agrees well with the in situ test results, and the relative errors are less than 10%. Water saturation and induced damage of the coal body in the parallel bedding direction are greater than that in the vertical bedding direction during the coal seam water injection process, which exhibits significant anisotropic characteristics. With the increasing water injection time, the induced damage of the coal body also increases near the water injection hole. Considering the inherent permeability arising with damage, it has a significant impact on both water saturation and induced damage, which also indicates that there is a strong interaction between water saturation and induced damage. The theoretical model reveals the coal damage mechanism of gas−liquid−solid multiphase coupling after coal seam water injection and provides a theoretical prediction of coal containing water characteristics in engineering practice.

1. INTRODUCTION

Before coal mining, coal seam water injection (CSWI) disrupts the balance of the original two-phase system of coal and gas, which forms a coal−gas−water three-phase new system. The interaction of different media in the system changes the physical and chemical properties, mechanical properties, and thermodynamic properties of coal.[1−3]

CSWI has great importance in reducing the generation of coal dust, reducing rock bursts, preventing coal and gas outbursts, and preventing spontaneous combustion. (1) Dust prevention mechanism: the wetting coal dust loses its flying ability. When a coal body breaks during mining, the wetting effect reduces the possibility that coal breaks into dust particles, which decreases the production of coal dust.[4−6] (2) Prevention of rock burst: high pressure water generates numerous cracks and damages the overall integrity of the coal body, which weakens its brittleness and enhances its plasticity. The changes in coal mechanical properties lead to the loss of coal burst tendency.[7,8] (3) Prevention of coal and gas outbursts: after wetting the coal body, its permeability significantly decreases, and the water-seal hinders the movement of gas, which courses that the gas emission velocity is significantly decreasing.[9,10] (4) Prevention of coal spontaneous combustion: after water injection, the thermal conductivity and heat capacity of the coal body increase, and it is difficult to raise the coal temperature, which suppresses the oxidation of floating coal in the goaf.[11]

Received: January 3, 2024
Revised: March 7, 2024
Accepted: March 13, 2024
Published: March 29, 2024

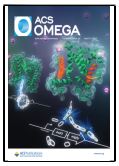

CSWI will induce damage and destruction of the coal body.[12] Phenomenological models are generally used to describe the damage and structural failure caused by directional microcracks in brittle materials. In these models, scalar internal variables are usually used to represent isotropic material damage, and second-order or fourth-order tensors are used to represent anisotropic damage.[13] Meanwhile, for microcrack growth, the physical mechanisms involved in microcrack growth, micro mechanical methods can also describe the macroscopic behavior of material damage.[14] However, these models are all based on dry, brittle materials. So, a new physical model is established for coupling water-containing brittle materials (coal and rock) with fluid mechanics to describe plastic deformation and material damage. Numerous scholars have conducted extensive theoretical research on containing water coal and rock, which is mainly divided into the following aspects: (1) numerical study of mechanical properties is used by classical elastic−plastic models for containing water coal and rock, but without considering induced anisotropic damage.[15] (2) The mechanical behavior of unsaturated coal and rock is studied without considering the coupling effect with fluid mechanics.[16,17] Therefore, it needs to establish a new model of the coupling effect of the damage mechanics between coal-rock and fluid, and in the new model, several physical characteristics are considered, which are the nonlinear pore elastic behavior of containing water coal, the relative permeability of water and gas variation with water saturation, damage and failure induced by water saturation, and the relationship between inherent permeability and coal damage.[18,19]

Based on the nonlinear pore elasticity theory and continuum mechanics,[20−22] an anisotropic pore elastic damage model is proposed with considering gas−liquid−solid coupling effect for CSWI.[23,24] Using a finite element method and fully coupled implicit algorithm, the time-varying characteristics of water saturation and induced damage are calculated and analyzed in the process of CSWI, which reveals the mechanism of water saturation and damage evolution of the coal body. This will provide a theoretical basis for studying the time-sensitive characteristics of CSWI.

2. IN SITU TEST OF CSWI

2.1. Water Injection Parameter Design. The CSWI test was conducted in a coal seam of 1303 working face of Zhaozhuang no. 2 well. The coal seam thickness is about 5.4 m, and the Proctor hardness of the coal seam is f = 0.6−1.02. Gas pressure in some areas reaches 1.3 MPa, and the average moisture content is about 1.45%. In the 1303 return airway, the water injection test area is selected and arranged within a range of 30−50 m. Three water injection boreholes are arranged: no. 1, no. 2, and no. 3, which is shown in Figure 1. Drilling and water injection parameters are listed in Table 1.

2.2. Measuring Point Arrangement. Before and after CSWI, the change of moisture content is an inherent manifestation of the water injection effect. And coal moisture content is measured through in-site sampling to comprehensively evaluate the CSWI effect. The groove sampling method is adopted to regularly measure the coal moisture content at different locations. Figure 2 shows the in-site sampling location (taking no. 1 water injection hole as an example).

2.3. Test Results and Analysis. The flow rate of CSWI is 1 m^3/h, and the duration is about 60 h. During the entire water injection process, coal samples are taken in real time around

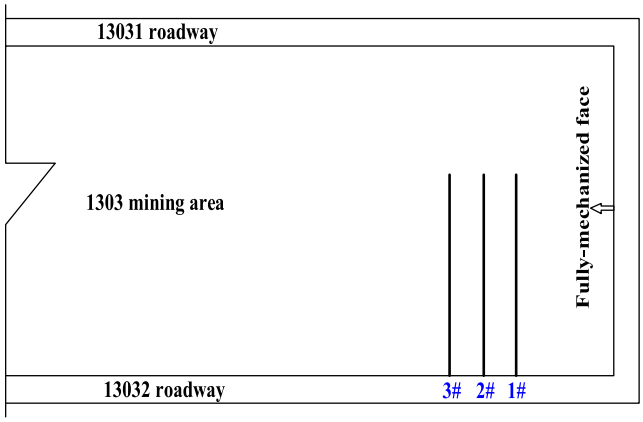

Figure 1. Schematic diagram of the water injection hole layout.

Table 1. Water Injection Parameters

drilling diameter (mm)	drilling length (m)	borehole spacing (m)	injection pressure (MPa)
45	60	10	8

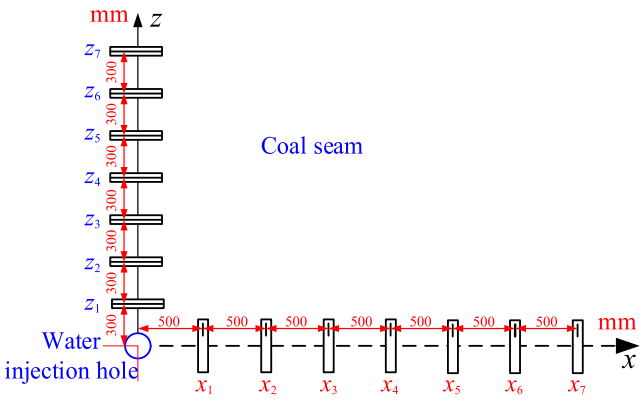

Figure 2. Layout of measuring points around 1 # water injection hole.

the borehole. The wetting radius of CSWI is determined by testing the moisture content of in-site sampling. The test results of moisture content are shown in Table 2 and Figure 3. According to the technical indicators of coal seam water injection, if the moisture content in coal seams reaches over 3.8% (or increases by over 1.8%), it can effectively prevent and control coal seam rockburst. Here, an increase of more than 1.8% (i.e., reaching 1.8% + 1.45% = 3.25%) in moisture content is necessary to achieve the technical indicators of CSWI, which effectively eliminates the risk of rock bursts. Wetting radius results are shown in Figure 4.

Figure 3 shows that after CSWI, the moisture content is smaller as the location is further from the injection hole. This reason is that water seeps and diffuses along coal seam pores from the injection hole, and the ability of water seepage and diffusion weakens along the radial direction. The farther away the position is, the less water there is, which results in a lower moisture content. With increasing CSWI time, the moisture content at the same location also gradually increases. This is because with the increasing injection amount, the amount of water reaching this location also increases, and moisture content also increases accordingly.

In order to determine the wetting radius after CSWI, it is necessary to consider the moisture content change. The coal

https://doi.org/10.1021/acsomega.4c00065
ACS Omega 2024, 9, 16400−16410

Table 2. Moisture Content of Coal Samples at Different Time Points

location		10 h		20 h		30 h		40 h		50 h		60 h	
x	z	x (%)	z (%)	x (%)	z (%)	x (%)	z (%)	x (%)	z (%)	x (%)	z (%)	x (%)	z (%)
x_1	z_1	4.8	4.5	5.4	5.1	5.7	5.5	5.9	5.8	6.1	6.0	6.3	6.1
x_2	z_2	3.3	2.8	4.0	3.8	4.6	4.3	5.2	4.7	5.7	5.2	6.0	5.5
x_3	z_3	2.5	2.1	3.1	2.8	3.8	3.4	4.4	3.8	5.1	4.3	5.5	4.6
x_4	z_4	2.0	1.6	2.5	2.2	3.1	2.6	3.6	3.0	4.3	3.4	4.8	3.8
x_5	z_5	1.7	1.5	2.0	1.7	2.5	2.0	3.0	2.4	3.4	2.7	3.9	3.1
x_6	z_6	1.5	1.45	1.6	1.5	1.9	1.7	2.2	1.9	2.6	2.2	3.1	2.5
x_7	z_7	1.45	1.45	1.5	1.45	1.6	1.5	1.8	1.6	2.1	1.8	2.4	2.0

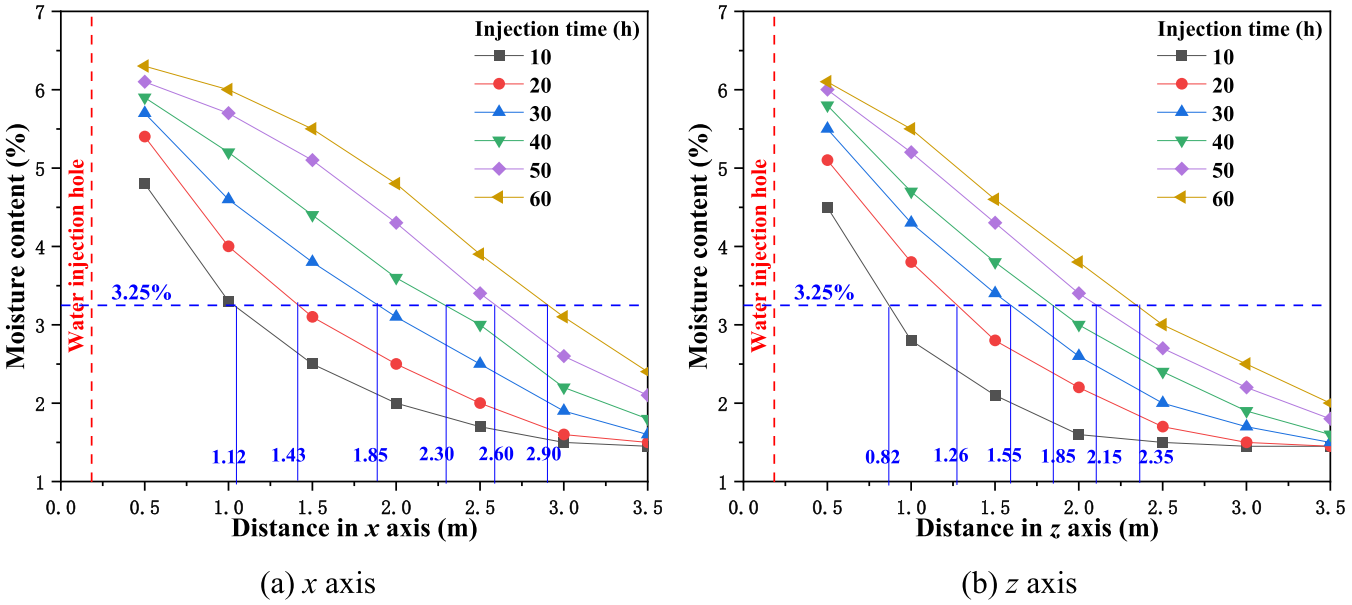

Figure 3. Moisture content curve of coal samples at different time points.

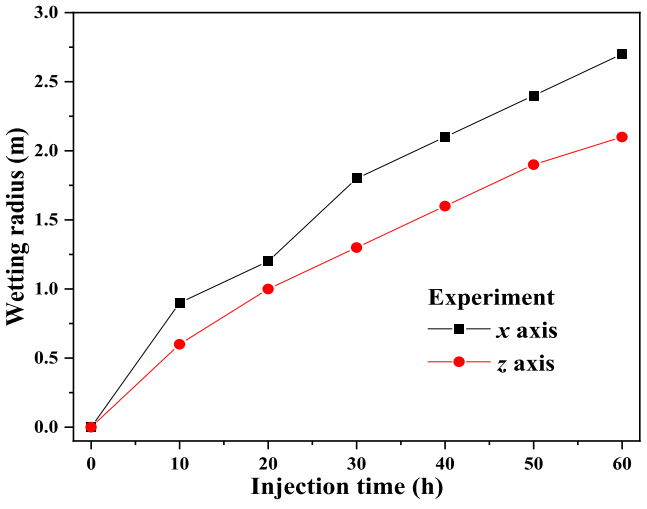

Figure 4. Time effect curve of the wetting radius with CSWI.

sample is taken using the groove method centered on the borehole, and when the moisture content reaches 3.25%, the location is used as a wetting radius. Figure 4 shows that the wetting radius of the borehole increases with CSWI time. In the initial stage, water diffuses within a small range of the borehole at a fast speed, which results in a large flow rate. With increasing CSWI time, the wetting range gradually increases, the velocity of water in the coal body slows down, the flow rate decreases, and the efficiency of water injection significantly decreases. Meanwhile, from Figure 4, it can be seen that there is a difference in the wetting radius of CSWI in the x direction (parallel bedding direction) and the z direction (vertical bedding direction) (Figure 4). The wetting radius in the x direction is significantly larger than that in the z direction. For example, when the water injection time is 60 h, the wetting radius can reach 2.7 m in the horizontal direction of the coal seam, while it is only 2.1 m in the vertical direction, which is because the physical properties of coal seams have anisotropic characteristics.

3. GAS−LIQUID−SOLID COUPLING CONTROL EQUATION FOR WATER INJECTION

3.1. Field Equation. During the CSWI process, the flow-solid quasi-static evolution control equation under gas/liquid saturation in a coal body includes the fluid mass conservation equation, fluid (gas/liquid) seepage equation, Fick diffusion equation, and coal body mechanical balance equation (water is represented by subscript "l", gas is represented by subscript "g").

The conservation equation for water and gas mass in coal can be expressed as[25]

$$\dot{m}_l = -\mathrm{div}(\mathbf{v}_l) \quad (1)$$

$$\dot{m}_g = -\mathrm{div}(\mathbf{v}_g) \quad (2)$$

https://doi.org/10.1021/acsomega.4c00065
ACS Omega 2024, 9, 16400−16410

where m_l and m_g, respectively, represent the water quality and gas quality in coal pores and $\mathbf{v}_l$ and $\mathbf{v}_g$, respectively, represent the water and gas flow velocity vectors in the coal body.

In coal seams, the seepage control equation for water and gas can be expressed as

$$\frac{\mathbf{v}_l}{\rho_l} = -\frac{k}{\mu_l} k_l^r \nabla p_l \tag{3}$$

$$\frac{\mathbf{v}_g}{\rho_g} = -\frac{k}{\mu_g} k_g^r \nabla p_g \tag{4}$$

where ρ_l and ρ_g are the water density and gas density in coal body, respectively; μ_l and μ_g are the water dynamic viscosity and gas dynamic viscosity, respectively; k_l^r is the water relative permeability; k_g^r is the gas relative permeability; and k is the coal inherent permeability.

The diffusion motion of water and gas in coal pores can be expressed using Fick's diffusion law as

$$\frac{\mathbf{v}_g}{\rho_g} - \frac{\mathbf{v}_l}{\rho_l} = -F_{ic}\frac{p_l}{p_g} \tag{5}$$

where p_l and p_g, respectively, represent the water pressure and gas pressure in the micro pores of the coal body and F_{ic} is the Fick diffusion coefficient.

During the CSWI process, the coal skeleton and fluid are in a quasi-static mechanical equilibrium state

$$\mathrm{div}(\sigma) = 0 \tag{6}$$

3.2. Nonlinear Pore Elastic Damage Model for CSWI.

For the multiphase coupled damage model of CSWI, it is assumed that the coal body is composed of two-phase saturation (liquid water and gas), incompressible liquid and solid matrix, and quasi-static problems (ignoring physical strength).

3.2.1. Nonlinear Pore Elastic Behavior. During the CSWI process, the pore structure of coal is full of water and gas. Here, based on the thermodynamic characteristics of saturated porous media, the constitutive model of isotropic materials is used to describe the elastic behavior of nonlinear pores in coal.[20] And for CSWI, its control equations under isothermal conditions are as follows

$$\mathrm{d}\sigma = E_s\,\mathrm{d}\varepsilon - b[S_l\,\mathrm{d}p_l + (1 - S_l)\mathrm{d}p_g]\delta \tag{7}$$

$$\mathrm{d}p_g = \frac{p_g}{\varphi_g}\left[-b\,\mathrm{d}\varepsilon_v + \left(\frac{\mathrm{d}m}{\rho}\right)_l\right] + \frac{p_g}{\varphi_g}\left(\frac{\mathrm{d}m}{\rho}\right)_g \tag{8}$$

$$\mathrm{d}p_c = \mathrm{d}p_g - \mathrm{d}p_l = -M_c\left[-bS_l\,\mathrm{d}\varepsilon_v + \left(\frac{\mathrm{d}m}{\rho}\right)_l\right] \tag{9}$$

where σ is the stress; E_s is the initial coal elastic stiffness; ε is the coal elastic strain; $S_l = \varphi_l/\varphi$ is water saturation; ε_V is the coal elastic volume strain; b is the coal Biot coefficient; φ_g is the gas volume fraction in the coal body; $\mathrm{d}m/\rho$ is the elastic change per unit volume of coal; p represents the fluid phase pressure; and p_c is the capillary pressure. E_c is the Biot modulus, which is related to water saturation (S_l) and capillary pressure (p_c)

$$E_c = -\frac{1}{\varphi_0 + \varepsilon_v}\left(\frac{\mathrm{d}p_c}{\mathrm{d}S_l}\right) \tag{10}$$

where φ_0 is the porosity of raw coal.

Capillary pressure (p_c) is related to the surface tension (γ) and pore radius (R)

$$p_c = \frac{2\gamma}{R} \tag{11}$$

3.2.2. Damage Characterization of Anisotropic Coal Body. The damage caused by CSWI is mainly reflected in the microcrack initiation and growth. Research has shown that microcracks induced by CSWI tend to develop in certain priority directions. The anisotropic damage elastic model is established under the premise of ignoring the plastic deformation of coal.[26] A second-order symmetric tensor ($\mathbf{D}$) is used to represent anisotropic coal damage, and its spectral decomposition form can be expressed as[27]

$$\mathbf{D} = \sum_{i=1}^{3} A_i V^i \otimes V^i \tag{12}$$

where A_i is the principal value and V^i is the vector. Based on this method, the influence of any microcrack in coal can be equivalent to three sets of orthogonal parallel microcracks.

Based on the basic principles of thermodynamics, a coupled damage model of pore elasticity in saturated (liquid/gas) coal is established. Here, it is assumed that the general thermodynamic formula in coal can be derived from strain ε, damage variable "$\mathbf{D}$" and change in fluid phase volume fraction $(\varphi-\varphi_0)_k$ (k = l, g)

$$\Gamma = \Gamma_s(\varepsilon, \mathbf{D}, (\varphi - \varphi_0)_k) + \Gamma_k \quad (k = l, g) \tag{13}$$

where Γ_s is the coal-free energy and Γ_k is the fluid-free enthalpy.

The conjugate force (F_C) related to damage can be expressed as

$$F_C = \frac{\partial \Gamma_s}{\partial \mathbf{D}}(\varepsilon, \mathbf{D}, (\varphi - \varphi_0)_k) \qquad (k = l, g) \tag{14}$$

The coal damage rate during CSWI can be determined by the pseudo-dissipative potential in the conjugate damage force space.[28] The conjugate damage force has a relationship with the deformation of the coal skeleton and the variation of porosity under the action of each fluid. It is assumed that the coal damage is induced by the deformation of the coal skeleton and affects the elastic performance. Therefore, the free energy of the coal skeleton can be expressed as porous elasticity and elastic damage

$$\Gamma_s(\varepsilon, \mathbf{D}, (\varphi - \varphi_0)_k) = \Gamma_s^{pe}(\varepsilon, (\varphi - \varphi_0)_k) + \Gamma_s^{ed}(\varepsilon, \mathbf{D}) \quad (k = l, g) \tag{15}$$

The free energy function is used to represent the effective elasticity of coal before water injection[29]

$$\Gamma_s^{ed}(\varepsilon, \mathbf{D}) = \zeta \mathrm{tr}(\varepsilon\cdot\mathbf{D}) + \frac{\lambda_0}{2}(\mathrm{tr}\,\varepsilon)^2 + \mu_0\,\mathrm{tr}(\varepsilon\cdot\varepsilon) + \alpha\,\mathrm{tr}\,\varepsilon\,\mathrm{tr}(\varepsilon\cdot\mathbf{D}) + 2\beta\,\mathrm{tr}(\varepsilon\cdot\varepsilon\cdot\mathbf{D}) \tag{16}$$

where λ_0 and μ_0 are the initial elastic constant of the coal body. The free energy function of coal containing pores and cracks is derived from micromechanics.[14] α and β indicate material

https://doi.org/10.1021/acsomega.4c00065
ACS Omega 2024, 9, 16400−16410

elastic degradation caused by the damage. In eq 16, the first item on the right represents the irreversible change caused by microcracks in unloading the coal body.

Research on coal/rock indicates that the anisotropic damage characteristics of coal/rock are related to tensile deformation. Therefore, the following specific form is used to describe the functional relationship between damage standards and equivalent tensile strain

$$f(\xi_d, \mathbf{D}) = \xi_d - C_0 - C_1 \operatorname{tr}\mathbf{D} = \sqrt{\varepsilon^e : \varepsilon^e} - C_0 - C_1 \operatorname{tr}\mathbf{D} = 0 \tag{17}$$

The tensile strain tensor (ε^e) can be calculated by spectral decomposition, which is expressed as[27]

$$\varepsilon^e = \sum_{i=1}^{3} H(\varepsilon_i)\varepsilon_i V^i \otimes V^i \tag{18}$$

where $H(\varepsilon_i)$ is the Heaviside function; C_0 is the initial damage threshold of coal body; and C_1 controls the coal damage rate. Meanwhile, it has been assumed that the coal damage rate tensor is coaxial with the tensile strain tensor

$$\dot{\mathbf{D}} = \dot{\chi}\frac{\partial f}{\partial \varepsilon^e} = \dot{\chi}\frac{\varepsilon^e}{\sqrt{\varepsilon^e : \varepsilon^e}} \tag{19}$$

where χ is the damage rate multiplier.

Here, only tr $\mathbf{D}$ in eq 17 indicates damage evolution. Moreover, taking the derivative of eq 17, the constitutive equation of the initial coal body can be obtained[29]

$$\sigma = \frac{\partial \Gamma_s^{ed}}{\partial \varepsilon} = \mathbf{B}^b(\mathbf{D}) : \varepsilon$$

$$\mathrm{d}\sigma = \mathbf{B}^b(\mathbf{D}) : \mathrm{d}\varepsilon + \left(\frac{\partial \mathbf{B}^b}{\partial \mathbf{D}} : \mathrm{d}\mathbf{D}\right) : \varepsilon = \mathbf{T}^b(\mathbf{D}) : \mathrm{d}\varepsilon \tag{20}$$

where $\mathbf{T}^b(\mathbf{D})$ is the tangent elastic tensor of coal damage under water injection conditions, which can be expressed as

$$\mathbf{T}^b = \mathbf{B}^b + \mathbf{U} \tag{21}$$

$$B^b_{ijkl} = \chi_0\delta_{ij}\delta_{kl} + \mu_0(\delta_{ik}\delta_{jl} + \delta_{il}\delta_{jk}) + \alpha(\delta_{ij}D_{kl} + D_{ij}\delta_{kl}) + \beta(\delta_{ik}D_{jl} + \delta_{il}D_{jk} + D_{ik}\delta_{jl} + D_{il}\delta_{jk}) \tag{22}$$

$$U_{ijkl} = \frac{1}{C_1 \operatorname{tr}\varepsilon^+\sqrt{\varepsilon^e : \varepsilon^e}}[\zeta\varepsilon^e + \alpha(\varepsilon_{pq}\varepsilon^e_{qp})\delta_{ij} + \alpha\varepsilon_{pp}\varepsilon^e_{ij} + 2\beta(\varepsilon_{iq}\varepsilon^e_{pj} + \varepsilon^e_{ip}\varepsilon_{pj})]\varepsilon^e_{kl} \tag{23}$$

The constitutive equation of coupled elastic damage with gas/liquid saturation conditions in coal is expressed as

$$\mathrm{d}\sigma = \mathbf{T}^b(\mathbf{D})\mathrm{d}\varepsilon - b[S_l\,\mathrm{d}p_l + (1 + S_l)\mathbf{d}p_g]\delta \tag{24}$$

The mechanical parameters are measured through triaxial compression conducted under diverse confining pressures and moisture contents.[26,30] A physical model is established for the boundary value problem mentioned above in the control equation. Implicit algorithms and Matlab programming are used to calculate the nonlinear problem of fluid−solid coupling during CSWI: (1) because the pore elasticity coefficient and relative permeability have a relationship with water saturation in a coal body, the nonlinear pore elasticity behavior is calculated and analyzed; (2) the nonlinear behavior is calculated and analyzed for the evolution of coal damage.

4. CSWI MODEL

4.1. Model and Initial Boundary Conditions. A physical model is established for CSWI to evaluate the characteristics of coal-induced damage. The geometric model size is large enough and does not affect the calculation results. The size in the z-axis direction is 50 times the drilling diameter of 45 mm (about 2.5 m) in the infinite boundary. The size in the x-axis direction is 5 m, as shown in Figure 5. In the model, u represents displacement; q is the water or gas flow rate, $q = \mathbf{v}\cdot\mathbf{n}$.

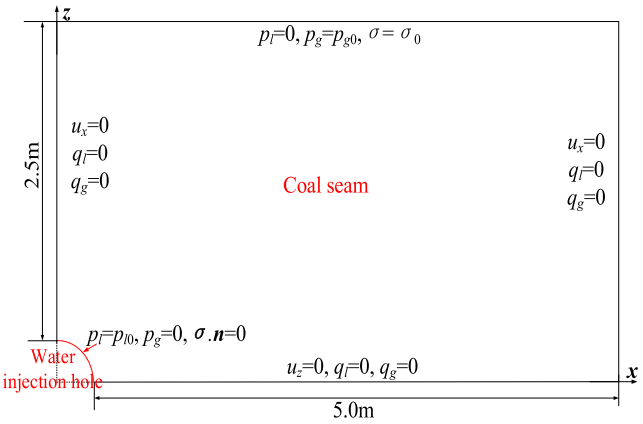

Figure 5. Geometry domain and boundary conditions of CSWI.

The initial gas in the coal body is saturated, and the initial stress and pressure values are estimated based on in-site measurements at the 1302 fully mechanized caving face of the Zhaozhuang no. 2 well. The basic boundary conditions are shown in Figure 5.

Water injection pressure: p_{l0} = 8 MPa; regional coal seam gas pressure: p_{g0} = 1.3 MPa; coal seam geostress (buried depth of about 450 m): σ_0 = 9.5 MPa.

4.2. Parameter Setting. The key parameters for CSWI are shown in Table 3 about coal and fluid characteristics.

Table 3. Key Parameters

symbol	parameters	values	unit
E_0	coal elastic modulus	3500	MPa
ν_0	coal Poisson's ratio	0.3	
φ_0	coal porosity	11.7%	
μ_l	water viscosity coefficient	1.4×10^{-3}	Pa·s
μ_g	gas viscosity coefficient	1.08×10^{-5}	Pa·s
ρ_l	water density	1000	kg/m^3
ρ_g	coal seam gas density (pressure 1.3 MPa)	9.32	kg/m^3
F_{ic}	diffusion coefficient	1.8×10^{-7}	m^2/s
k_0	intrinsic permeability	1.0×10^{-9}	m^2
B	biot coefficient	1.0	

4.2.1. Relationship between Water Saturation and Capillary Pressure. After CSWI, water enters the pore structure. Research has shown that water saturation is related to capillary pressure p_c (Figure 6), and its approximate relationship can be expressed as[31]

https://doi.org/10.1021/acsomega.4c00065
ACS Omega 2024, 9, 16400−16410

$$S_l = \frac{0.56}{0.56 + 0.16 p_c^{1.01}} \quad (25)$$

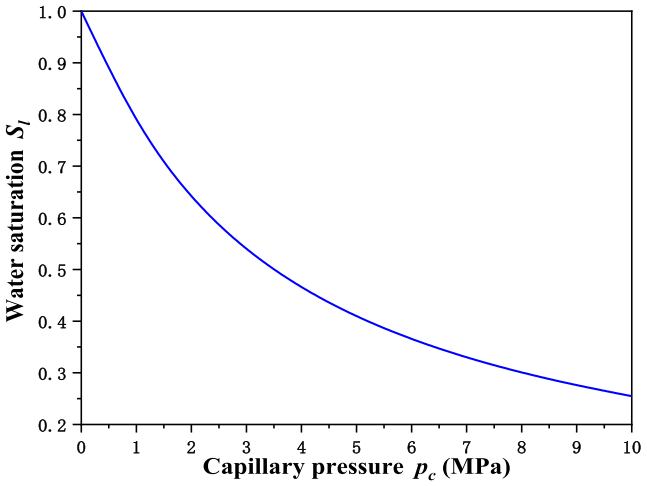

Figure 6. Relationship curve between water saturation and capillary pressure of coal body.

4.2.2. Relationship between Water Saturation and Relative Permeability. After CSWI, water and gas are present in the coal body. The effective permeability of the coal seam is the ability to allow each relative fluid to pass through when gas and liquid fluids coexist. The coal pore determines the water and gas permeability characteristics, so the permeability changes of water and gas in the coal seam during should be considered the CSWI process.[32]

The test process of gas and water relative permeability is as follows: (1) after the coal sample is put into the core gripper, water is injected from one end under a certain pressure. When the outlet flow rate stabilizes, the water phase permeability is calculated. (2) Using gas to drive water, the bound water saturation is established for the coal sample, and the effective permeability of the gas phase is measured in the bound water state. (3) Gas and water with a certain proportion are injected into the coal sample, and after the flow stabilizes, it needs to measure the inlet and outlet pressure difference, gas and water flow rates, and so on. (4) The proportion of water gradually increases, and when the gas phase relative permeability value is less than 0.005, the water phase permeability is measured.

Experiments have shown that with increasing water saturation in coal, the water's relative permeability first grows slowly and then sharply. As water saturation in the coal increases, the gas's relative permeability declines rapidly, as shown in Figure 7.

The relationships of the relative permeability and water saturation in coal are approximated as[33,34]

$$k_k^r = \frac{1}{1 + [35(1 - S_l)]^{1.5}} \quad (26)$$

$$k_g^r = \frac{1}{1 + (3S_l)^{2.7}} \quad (27)$$

4.2.3. Relationship between Water Saturation and Moisture Content. The moisture content of coal (w) can be expressed as

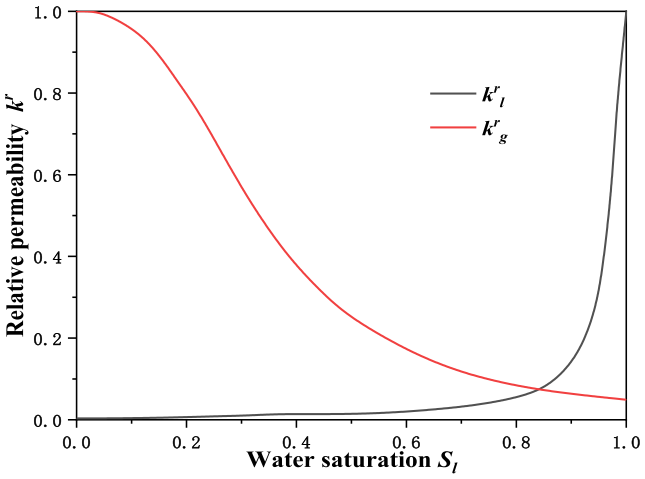

Figure 7. Relationship curve between water saturation and relative permeability of coal body.

$$w = \frac{m_l}{m_l + m_c} \quad (28)$$

Water saturation during the CSWI process refers to the ratio of the water volume in a coal body (V_l) to the water maximum volume that can be accommodated in the pores (pore volume V_φ), Namely,

$$S_l = \frac{V_l}{V_\varphi} \quad (29)$$

Water is an incompressible fluid, then

$$V_l = \frac{m_l}{\rho_l} \quad (30)$$

The mass (m_c) and pore volume (V_φ) of coal can be represented as

$$m_c = \rho_c V \quad (31)$$

$$V_\varphi = V\varphi \quad (32)$$

where ρ_c is the coal density and V is the coal volume.

From eqs 28−32, the relationship between the moisture content and water saturation can be obtained

$$S_l = \frac{\rho_c w}{\rho_l \varphi (1 - w)} \quad (33)$$

5. CALCULATION AND DISCUSSION OF NONLINEAR ELASTIC DAMAGE IN CSWI

5.1. Verification of Calculation Results. For verifying the accuracy of the calculation results using the nonlinear elastic model, the parameters given in Section 4 are used to numerically calculate water saturation curves of the coal seam along the x-axis and z-axis directions at different water injection times, as in Figures 8a and 9a. The moisture content curves converted by eq 33 are shown in Figures 8b and 9b.

From Figures 8 and 9, it can be seen that both in the x-axis and z-axis directions, water saturation and moisture content have the same radial variation trend after water injection. The distance away from the injection hole is further, and the water saturation and moisture content are smaller. Compared with that in the x-axis direction, water saturation and moisture content in the z-axis direction at the same position and time

https://doi.org/10.1021/acsomega.4c00065
ACS Omega 2024, 9, 16400−16410

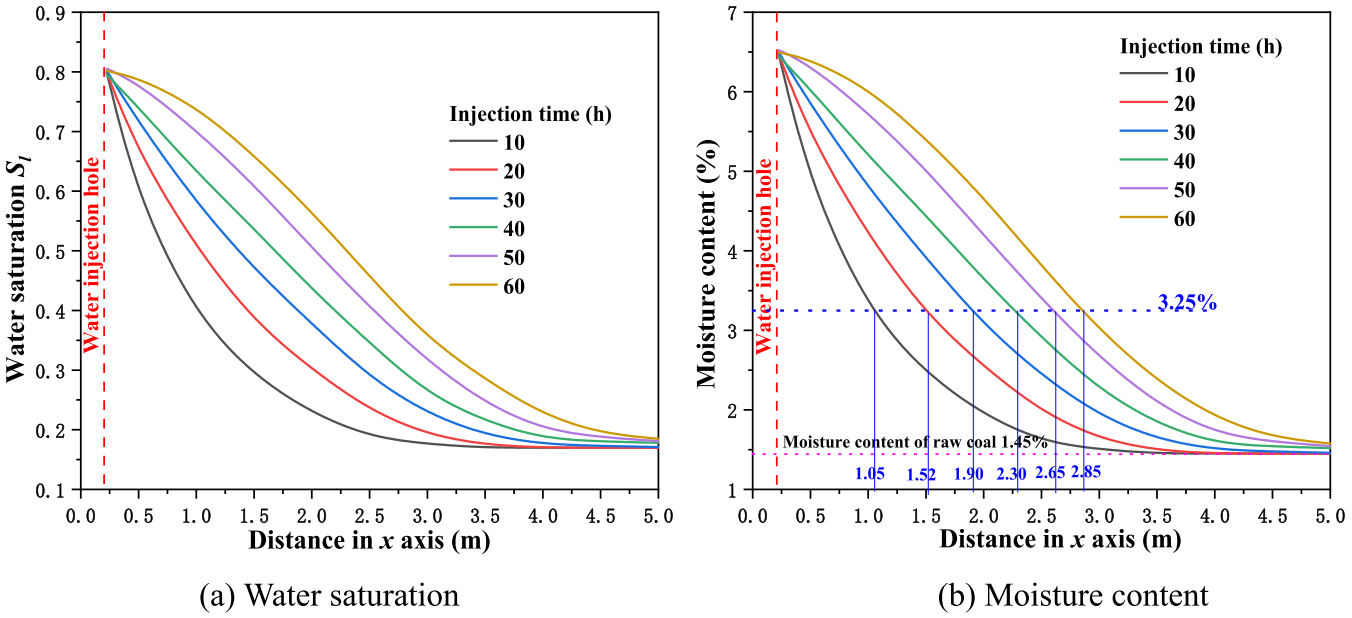

Figure 8. Water saturation and moisture content variation curve in the horizontal direction (x-axis).

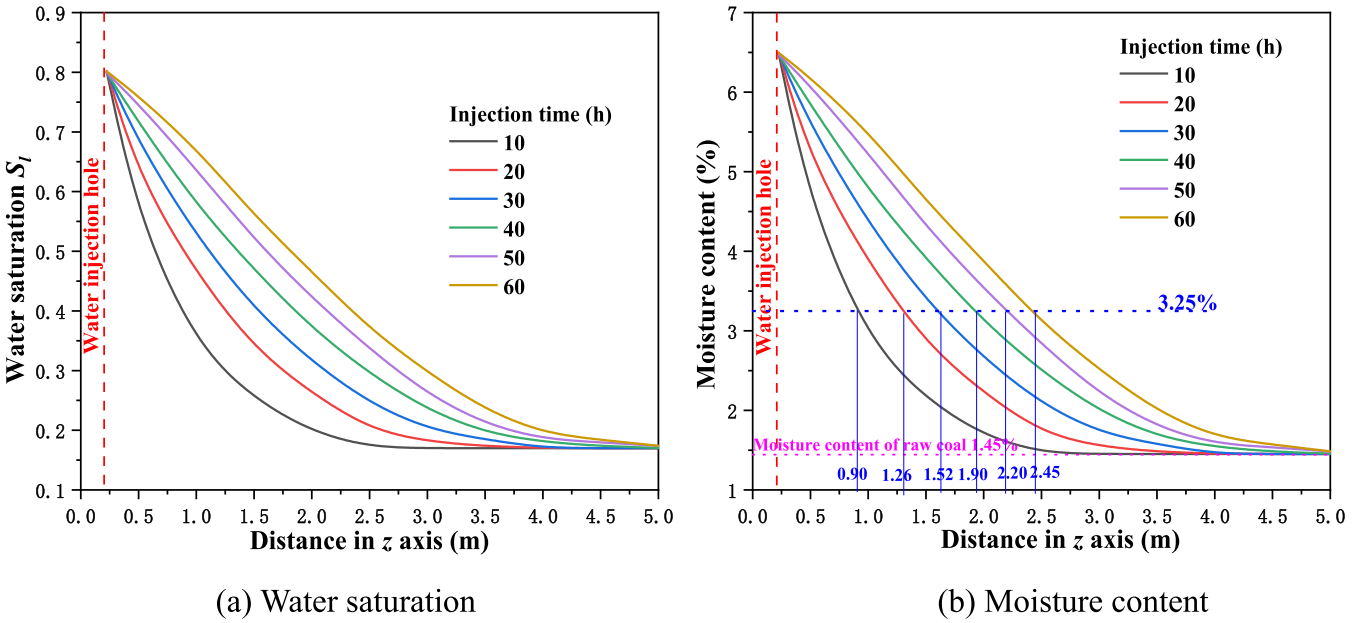

Figure 9. Water saturation and moisture content variation curve in the horizontal direction (z-axis).

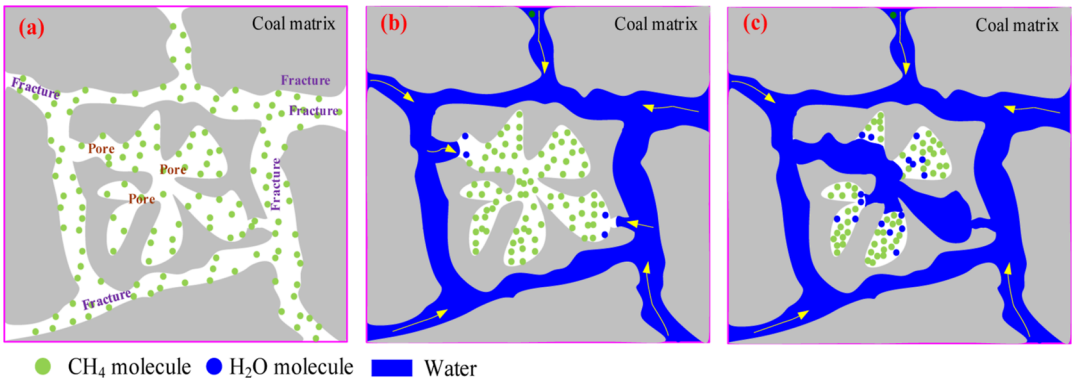

Figure 10. Schematic diagram of the water−gas interaction during the CSWI process.

https://doi.org/10.1021/acsomega.4c00065
ACS Omega 2024, 9, 16400−16410

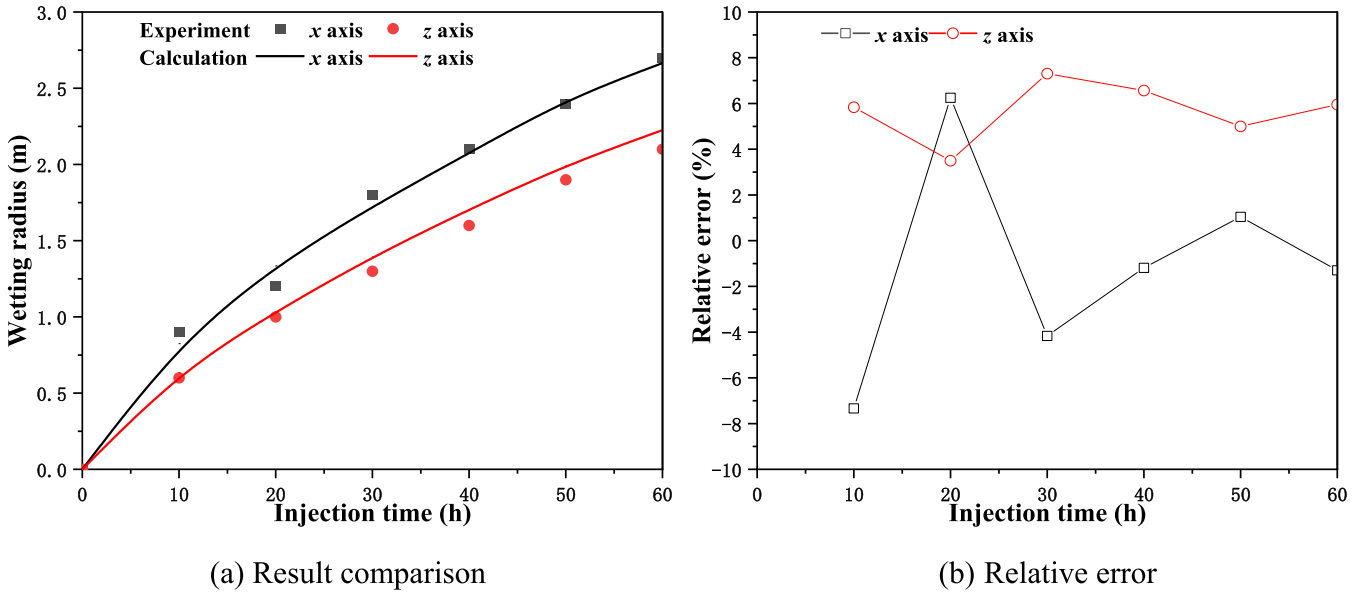

(a) Result comparison (b) Relative error

Figure 11. Comparison between the calculation and measured results of the wetting radius.

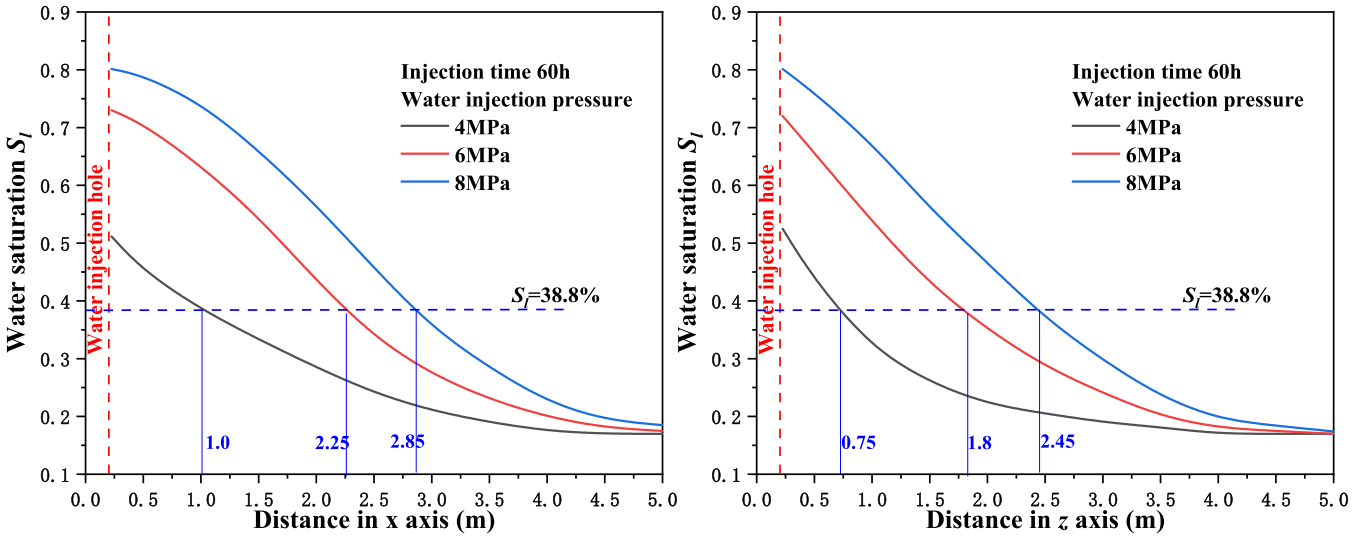

(a) *x* axis (b) *z* axis

Figure 12. Influence of injection pressure on water saturation.

are relatively smaller, which is due to the anisotropic characteristics of the coal seam.

Meanwhile, from Figures 8a and 9a, it can also be seen that even if a large amount of water enters the coal body near the injection hole, water saturation cannot reach 1.0 but remains stable at around 0.8. Because there is gas in the coal pore structure, the gas blocked by water in the pores cannot be discharged and occupies a certain pore volume.

Before CSWI, there is much gas in the pores and cracks of the coal body (Figure 10a). After the beginning of the water injection, water first enters relatively larger cracks (Figure 10b), and as the water injection time increases, water in coal cracks gradually diffuses into relatively smaller pores. Moreover, with increasing gas pressure in the micropores, liquid water is difficult to enter (as shown in Figure 10c), which also results in water saturation being less than 1.0 for coal bodies containing gas.

According to the technical indicators of CSWI compliance (with a moisture content of 3.25%), Figures 8b and 9b, the wetting radii are shown in Figure 11 in the *x* and *z* directions.

Figure 11 indicates that under a water injection pressure of 8 MPa, both in the *x*-axis and *z*-axis directions, the wetting radii calculated by the nonlinear elastic pore damage model are consistent with in-site test results, and relative errors are less than 10%, which indicates that the nonlinear pore elastic damage model is feasible for multiphase (gas−liquid−solid) coupled damage analysis.

5.2. Analysis of Anisotropic Damage Characteristics of CSWI. *5.2.1. Analysis of the Influence of Water Injection Pressure on Coal Wettability.* For the effect of water injection pressure on the coal wettability, the changes in water saturation of the coal body in the horizontal and vertical directions are calculated under water injection pressures of 4, 6, and 8 MPa.

https://doi.org/10.1021/acsomega.4c00065
ACS Omega 2024, 9, 16400−16410

Figure 12 shows that under different water injection pressures, water saturation along the horizontal and vertical directions has a similar pattern; that is, water saturation gradually decreases with increasing distance. Meanwhile, water injection pressure has a great influence on the water saturation of the coal body. The greater the water injection pressure, the higher the water saturation at the same location. This is because water injection pressure drives the flow of water in the coal body. And the larger the pressure, the stronger the fluidity of water, and the farther it moves at the same time. Moreover, the larger the pressure, the greater the amount of water that overcomes gas pressure and capillary pressure and enters the pores. Therefore, water saturation at the same location is also higher, and the coal-wetting radius is also bigger.

5.2.2. Analysis of the Influence of Water Injection Time on Coal Wettability. Under the injection pressure of 8 MPa and with the inherent permeability remaining constant, the nonlinear pore elastic damage coupling model is used to calculate the horizontal and vertical damage evolution during the CSWI process, as shown in Figure 13.

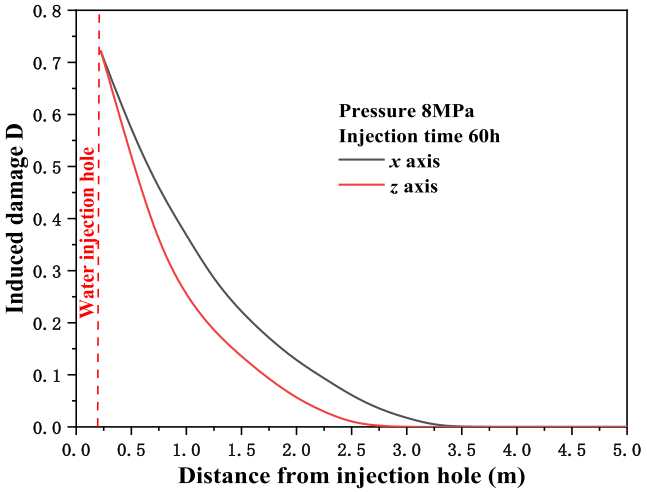

Figure 13. Induced damage of the coal body after CSWI.

During the process of CSWI, due to the influence of geostress, the maximum tensile strain is vertical to horizontal stress, which causes the damage in the x-axis direction to be larger than that in the z-axis direction.

Figure 14 shows the distribution of coal-induced damage in the horizontal and vertical directions at different injection times (40, 60, and 80 h) under the injection pressure of 8 MPa. From Figure 14, it can be seen that whether in the horizontal or vertical direction, the damage of the coal body decreases with the distance increasing from the water injection hole. Moreover, as the water injection time increases, the amount of water entering the coal seam increases, and damage and destruction of the coal body increase near the water injection hole. Compared with induced damage in the horizontal direction, the degree of damage and destruction in the vertical direction at the same time and location is relatively smaller.

5.2.3. Analysis of the Influence of Inherent Permeability on Coal Wettability. From a physical perspective, the development of microcracks during the water injection process alters the pore structure of coal, which causes a corresponding increase in the coal's inherent permeability.

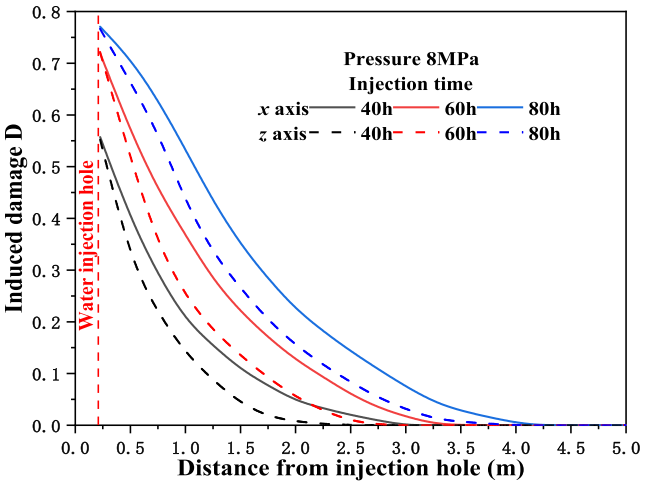

Figure 14. Distribution of horizontal and vertical damage of coal seam at different injection times.

Moreover, directional microcracks exhibit anisotropic characteristics in coal, which in turn induces the anisotropy of the inherent permeability. Therefore, the inherent permeability and anisotropy is simplified as a relationship with the damage tensor, that is,

$$k = k_0\left[1 + 99\frac{\mathrm{tr}(\mathbf{D})}{D_{\mathrm{pv}}}\right] \tag{34}$$

where k_0 is the initial permeability of the coal body and D_{pv} is the damage factor corresponding to the peak stress of uniaxial compression of the coal body.

Figures 15 and 16 respectively, show water saturation and induced damage curves of the coal body in the x-axis and z-axis

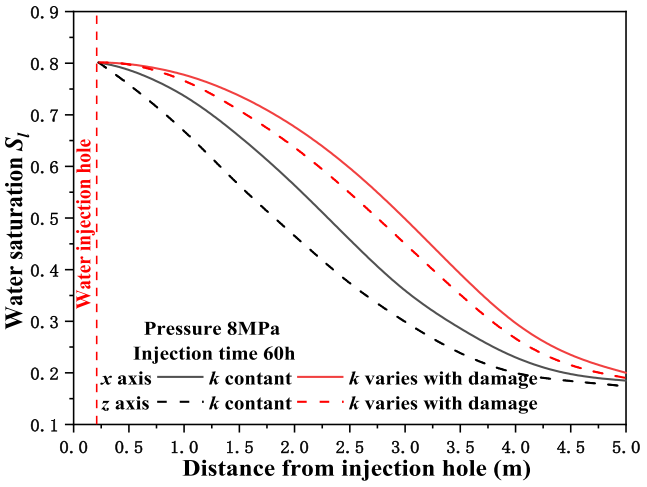

Figure 15. Influence of water saturation with constant inherent permeability and inherent permeability variation with damage.

directions after 60 h of water injection. At the same time, a comparative analysis is conducted on water saturation and induced damage as the constant inherent permeability and inherent permeability variation with damage.

Figure 15 shows that compared with the calculated results of constant inherent permeability, as the inherent permeability variation with damage, water saturation of the coal body increases in the x-axis and z-axis directions. The variable

https://doi.org/10.1021/acsomega.4c00065
ACS Omega 2024, 9, 16400−16410

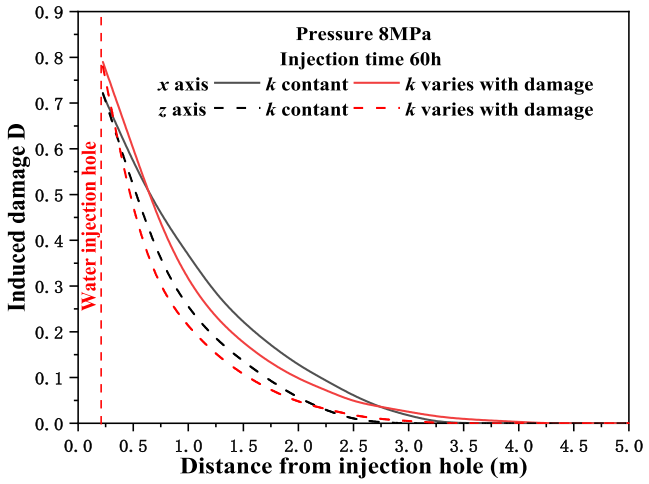

Figure 16. Influence of induced damage with constant inherent permeability and inherent permeability variation with damage.

inherent permeability has a significant impact on the water saturation of the coal body.

Figure 16 shows that although the effect of induced damage with constant and variable inherent permeability is less obvious than that of water saturation, the maximum value of induced damage will increase (0.72−0.79) with variable inherent permeability. In a word, the damage evolution has an intense interaction with water saturation during the CSWI process.

6. CONCLUSIONS

CSWI is of great significance in reducing coal dust, reducing rock burst pressure, preventing coal and gas outbursts, and preventing spontaneous combustion. During the water injection process, water not only infiltrates the coal body but also causes damage and destruction to the coal body. Based on the nonlinear pore elasticity theory and continuum damage mechanics, a nonlinear pore elastic damage model was proposed, and the gas−liquid−solid multiphase coupling damage of CSWI is calculated using Matlab programming. The results are compared and analyzed with the in situ measurement results. The following conclusions have been drawn.

1 Combined with the change trend and quantitative result analysis, the time-varying characteristics of the wetting radius calculated by the nonlinear pore elastic damage model are well agreed with the in situ test results of CSWI, and the relative errors are less than 10%, which fully verifies the reliability of the model.
2 After CSWI, water saturation and induced damage of the coal body decrease radially and exhibit anisotropic characteristics, which are more significant in the horizontal direction (bedding direction, *x*-axis) than in the vertical direction (vertical bedding direction, *z*-axis).
3 As the water injection time increases, the degree of damage and destruction near the water injection hole increases, but the induced damage in the *x*-axis direction is more obvious than that in the *z*-axis direction at the corresponding position.
4 In the process of CSWI, there is a strong interaction between water saturation and damage evolution. Compared with the constant inherent permeability of coal seams, considering variable inherent permeability has a greater impact on water saturation and induced damage, and the damage near the water injection hole is more significant.

In the new model established in this paper, the mechanical behavior is simplified as elastic damage. In fact, plastic deformation may be important in a coal body, so in further research, the constitutive model should be extended to plastic damage coupling.

■ ASSOCIATED CONTENT

Data Availability Statement

The data used to support the findings of this study are included within the article.

■ AUTHOR INFORMATION

Corresponding Author

Yuehui Liang − *School of Safety Science and Engineering, Anhui University of Science and Technology, Huainan, Anhui 232001, China;* orcid.org/0009-0003-0824-7884; Email: AUSTlyh@163.com

Authors

Biming Shi − *School of Safety Science and Engineering, Anhui University of Science and Technology, Huainan, Anhui 232001, China*

Jiwei Yue − *School of Safety Science and Engineering, Anhui University of Science and Technology, Huainan, Anhui 232001, China; State Key Laboratory Cultivation Base for Gas Geology and Gas Control, Henan Polytechnic University, Jiaozuo, Henan 454000, China*

Chengcheng Zhang − *School of Safety Science and Engineering, Anhui University of Science and Technology, Huainan, Anhui 232001, China*

Qijun Han − *School of Safety Science and Engineering, Anhui University of Science and Technology, Huainan, Anhui 232001, China;* orcid.org/0009-0001-5466-1483

Complete contact information is available at: https://pubs.acs.org/10.1021/acsomega.4c00065

Notes

The authors declare no competing financial interest.

■ ACKNOWLEDGMENTS

The authors are grateful for financial support from the National Natural Science Foundation of China (U23A20601), the Anhui Provincial Natural Science Foundation (2308085QE152), and the State Key Laboratory Cultivation Base for Gas Geology and Gas Control (Henan Polytechnic University) (no. WS2022B03). The authors also appreciate the editor and the anonymous reviewers for their careful reviews of this paper.

■ REFERENCES

(1) Yan, J. J.; Wang, F.; Li, Y. C.; Gao, Y. B.; Li, Z. G.; Liu, H. W. A feasibility study of coal seam water injection processes: the effects of coal porosity and mass flow rates of injected water on wetting radii. *Energy Fuels* **2020**, *34* (12), 16956−16967.

(2) Lin, X. L.; Liu, Z.; Geng, N.; Hu, P.; Gu, Q. B. Optimization and application of water injection process in gas-bearing coal seam. *Processes* **2023**, *11* (10), 3003.

(3) Fan, C. J.; Xu, L. J.; Elsworth, D.; Luo, M. K.; Liu, T.; Li, S.; Zhou, L. J.; Su, W. W. Spatial−temporal evolution and countermeasures for coal and gas outbursts represented as a dynamic system. *Mec. Des. Roches* **2023**, *56* (9), 6855−6877.

https://doi.org/10.1021/acsomega.4c00065
ACS Omega 2024, 9, 16400−16410

(4) Zhao, L. J.; Li, Y.; Duan, H. F. Field experimental study on comprehensive dust control technology in fully mechanized caving face of extra thick coal seam. *Therm. Sci.* **2023**, *27* (1 Part B), 679−686.
(5) Zhou, Q.; Qin, B. T. Coal dust suppression based on water mediums: a review of technologies and influencing factors. *Fuel* **2021**, *302*, 121196.
(6) Zhang, K. X.; Zhang, J.; Wei, J. P.; Ren, T.; Xu, X. Y. Coal seam water infusion for dust control: a technical review. *Environ. Sci. Pollut. Res.* **2019**, *26*, 4537−4554.
(7) Liu, X. F.; Xu, G.; Zhang, C.; Kong, B.; Qian, J. F.; Zhu, D.; Wei, M. Y. Time effect of water injection on the mechanical properties of coal and its application in rockburst prevention in mining. *Energies* **2017**, *10* (11), 1783.
(8) Zhang, J. F.; Wang, R. Y.; Yang, F. F.; Lei, W. L.; Feng, B. Y.; Zheng, C.; Zhang, J. J.; Miao, Z. Q. Discussion on the mechanism of coal and gas outburst prevention and control by the coal seam water injection. *IOP Conf. Ser. Earth Environ. Sci.* **2019**, *252* (5), 052090.
(9) Wang, C. J.; Li, X. W.; Liu, L. T.; Tang, Z. X.; Xu, C. H. Dynamic effect of gas initial desorption in coals with different moisture contents and energy-controlling mechanism for outburst prevention of water injection in coal seams. *J. Pet. Sci. Eng.* **2023**, *220*, 111270.
(10) Xu, L. J.; Fan, C. J.; Luo, M. K.; Li, S.; Han, J.; Fu, X.; Xiao, B. Elimination mechanism of coal and gas outburst based on geo-dynamic system with stress−damage−seepage interactions. *Int. J. Coal Sci. Technol.* **2023**, *10* (1), 74.
(11) Liu, Z.; Wang, W. Y.; Yang, H.; Zhao, D. W.; Wang, W. D. Experimental study on spontaneous imbibition characteristics of coal based on fractal theory. *Adv. Powder Technol.* **2020**, *31* (5), 1994−2004.
(12) Deng, B. Z.; Zhang, D. M.; Chen, J. Q. Dilation behavior and acoustic emission response to water/CO_2 injection-induced shear fracturing in coal seams. *J. Nat. Gas Sci. Eng.* **2021**, *94*, 104105.
(13) Shao, J. F.; Rudnicki, J. W. A microcrack based continuous damage model for brittle geomaterials. *Mech. Mater.* **2000**, *32*, 607−619.
(14) Pensèe, V.; Kondo, D.; Dormieux, L. A micromechanical analysis of anisotropic damage in brittle materials. *J. Eng. Mech. Div.* **2002**, *128*, 889−897.
(15) Liu, Z.; Hu, P.; Yang, H.; Yang, W. Z.; Gu, Q. B. Coupling mechanism of coal body stress−seepage around a water injection borehole. *Sustainability* **2022**, *14* (15), 9599.
(16) Yu, Y. B.; Xin, Q. L.; Cheng, W. M.; Rui, J.; Zhang, X. Numerical simulation study on the seepage characteristics of coal seam infusion effected by mining-induced stress. *Bull. Eng. Geol. Environ.* **2021**, *80* (12), 9015−9028.
(17) Yang, H.; Cheng, W. M.; Liu, Z.; Wang, W. D.; Zhao, D. W.; Yang, W. Z. Study on the dynamic evolution law the effective stress in the coal seam water infusion process based on fractal theory. *Fractals* **2020**, *28* (05), 2050086.
(18) Wang, G.; Guo, Y. Y.; Wang, P. F.; Li, W. X.; Wu, M. M.; Sun, L. L.; Cao, J. J.; Du, C. G. A new experimental apparatus for sudden unloading of gas-bearing coal. *Bull. Eng. Geol. Environ.* **2020**, *79* (2), 857−868.
(19) Yue, J. W.; Wang, Z. F.; Dong, J. X.; Wang, C. G.; Shen, X. J. Law of water migration during spontaneous imbibition in loaded coal and its influence mechanism. *J. China Coal Soc.* **2022**, *47* (11), 4069−4082.
(20) Coussy, O.; Eymard, R.; Lassabatere, T. Constitutive Modeling of Unsaturated Drying Deformable Materials. *J. Eng. Mech.* **1998**, *124* (6), 658−667.
(21) Wang, K.; Guo, Y. Y.; Du, F.; Dong, H. Z.; Xu, C. Effect of the water injection pressure on coal permeability based on the pore-fracture fractal characteristics: an experimental study. *Greenhouse Gases: Sci. Technol.* **2022**, *12* (1), 136−147.
(22) Yue, J. W.; Ma, Y. K.; Wang, Z. F.; Zhang, X.; Wang, L.; Shen, X. J. Characteristics of water migration during spontaneous imbibition in anisotropic coal. *Energy* **2023**, *263*, 126054.
(23) He, L. W.; Jin, Z. H. A local thermal nonequilibrium poroelastic theory for fluid saturated porous media. *J. Therm. Stresses* **2010**, *33* (8), 799−813.
(24) Zhang, C.; Bai, Q. S.; Han, P. H.; Wang, L.; Wang, X. J.; Wang, F. T. Strength weakening and its micromechanism in water−rock interaction, a short review in laboratory tests. *Int. J. Coal Sci. Technol.* **2023**, *10* (1), 10.
(25) Shao, J. F.; Ata, N.; Ozanam, O. Study of desaturation and resaturation in brittle rock with anisotropic damage. *Eng. Geol.* **2005**, *81*, 341−352.
(26) Chiarelli, A. S.; Shao, J. F.; Hoteit, N. Modeling of elastoplastic damage behavior of a claystone. *Int. J. Plast.* **2003**, *19*, 23−45.
(27) Ortiz, M. A constitutive theory for the inelastic behavior of concrete. *Mech. Mater.* **1985**, *4*, 67−93.
(28) Xiao, B.; Guo, D. X.; Li, S.; Xiong, S. Z.; Jing, Z. Y.; Feng, M. F.; Fu, X.; Zhao, Z. H. Rare Earth Element Characteristics of Shales from Wufeng−Longmaxi Formations in Deep-Buried Areas of the Northern Sichuan Basin, Southern China: Implications for Provenance, Depositional Conditions, and Paleoclimate. *ACS Omega* **2024**, *9* (2), 2088−2103.
(29) Halm, D.; Dragon, A. A model of anisotropic damage by mesocrack growth; unilateral effect. *Int. J. Damage Mech.* **1996**, *5*, 384−402.
(30) Wang, K.; Zhao, E. B.; Guo, Y. Y.; Du, F.; Ding, K. Effect of loading rate on the mechanical and seepage characteristics of gas-bearing coal−rock and its mechanical constitutive model. *Phys. Fluids* **2024**, *36* (2), 026606.
(31) Zheng, B.; Chen, J. J.; Wei, B.; Zhi, Y. F. Experimental study of capillary pressure-saturation relationship for immiscible liquids in porous media. *J. Hydrodyn.* **2005**, *20* (5), 665−672.
(32) Yue, J. W.; Wang, Z. F.; Shi, B. M.; Dong, J. X.; Shen, X. J. Interaction mechanism of water movement and gas desorption during spontaneous imbibition in gas-bearing coal. *Fuel* **2022**, *318*, 123669.
(33) Cheng, W. M.; Liu, Z.; Yang, H.; Wang, W. Y. Non-linear seepage characteristics and influential factors of water injection in gassy seams. *Exp. Therm. Fluid Sci.* **2018**, *91*, 41−53.
(34) Liu, Z.; Wang, W. Y.; Cheng, W. M.; Yang, H.; Zhao, D. W. Study on the seepage characteristics of coal based on the Kozeny-Carman equation and nuclear magnetic resonance experiment. *Fuel* **2020**, *266*, 117088.

https://doi.org/10.1021/acsomega.4c00065
ACS Omega 2024, 9, 16400−16410